Molecular Therapy
Nucleic Acids
Original Article

Effective gene therapy for metachromatic leukodystrophy achieved with minimal lentiviral genomic integrations

Lucas Tricoli,[1] Sunetra Sase,[2] Julia L. Hacker,[2] Vi Pham,[3,4,5] Maxwell Chappell,[1] Laura Breda,[1] Stephanie N. Hurwitz,[6,7] Naoto Tanaka,[1] Carlo Castruccio Castracani,[1] Amaliris Guerra,[1] Zhongqi Hou,[2] Lars Schlotawa,[8,9] Karthikeyan Radhakrishnan,[10] Matthew Hogenauer,[11] Aoife Roche,[11] John Everett,[11] Frederic Bushman,[11] Peter Kurre,[1,4,7] Rebecca Ahrens-Nicklas,[3,4] Laura A. Adang,[2,12] Adeline L. Vanderver,[2,11] and Stefano Rivella[1,4,13,14,15,16,17]

[1]Department of Pediatrics, Division of Hematology, Children's Hospital of Philadelphia, Philadelphia, PA, USA; [2]Department of Pediatrics, Division of Neurology, Children's Hospital of Philadelphia, Philadelphia, PA, USA; [3]Department of Pediatrics, Division of Human Genetics, Children's Hospital of Philadelphia, Philadelphia, PA, USA; [4]University of Pennsylvania, Perelman School of Medicine, Philadelphia, PA, USA; [5]Cell and Molecular Biology affinity group (CAMB), University of Pennsylvania, Philadelphia, PA, USA; [6]Department of Pathology and Laboratory Medicine, University of Pennsylvania, Philadelphia, PA, USA; [7]Comprehensive Bone Marrow Failure Center, CHOP, Philadelphia, PA, USA; [8]University Medical Centre Göttingen, Göttingen, Germany; [9]Fraunhofer Institute for Translational Medicine – Translational Neuroinflammation and Automated Microscopy, Göttingen, Germany; [10]Bielefeld University, Bielefeld, Germany; [11]Department of Microbiology, Perelman School of Medicine, University of Pennsylvania, Philadelphia, PA, USA; [12]Department of Neurology, Perelman School of Medicine, University of Pennsylvania, Philadelphia, PA, USA; [13]Hospital of the University of Pennsylvania, Philadelphia, PA, USA; [14]RNA Institute, University of Pennsylvania, Philadelphia, PA, USA; [15]Institute for Regenerative Medicine, University of Pennsylvania, Philadelphia, PA, USA; [16]Penn Center for Musculoskeletal Disorders, CHOP, Philadelphia, PA, USA; [17]Raymond G. Perelman Center for Cellular and Molecular Therapeutics-CHOP, Philadelphia, PA, USA

Metachromatic leukodystrophy (MLD) is a fatal lysosomal storage disease characterized by the deficient enzymatic activity of arylsulfatase A (ARSA). Combined autologous hematopoietic stem cell transplantion (HSCT) with lentiviral (LV)-based gene therapy has great potential to treat MLD. Achieving the optimal balance between high enzyme production for therapeutic efficacy and maintaining a low vector copy number (VCN) is crucial. Insufficient enzyme levels can lead to the progression of motor symptoms, undermining treatment goals. Conversely, elevated VCN increases the risk of genotoxicity, which poses safety concerns, and contributes to higher production costs, making the therapy less accessible. Striking this balance is essential to maximize clinical benefit while minimizing risks and costs. To address this need, we increased the expression of ARSA cDNA at single integration by generating novel LVs, optimizing ARSA expression and enhancing safety. In addition, our vectors achieved optimal transduction in mouse and human hematopoietic stem cells (HSCs) with minimal multiplicity of infection (MOI). Our top-performing vector (EA1) showed at least 4× more ARSA activity than the currently US and European Union (EU)-approved vector and a superior ability to secrete vesicle-associated ARSA, a critical modality to transfer functional enzymes from microglia to oligodendrocytes. Three-month-old *Arsa*-knockout (KO) MLD mice transplanted with *Arsa*-KO bone marrow (BM) cells transduced with 0.6 VCN of EA1 demonstrated behavior and CNS histology matching wild-type (WT) mice. Our novel vector boosts efficacy while improving safety as a robust approach for treating MLD patients.

INTRODUCTION

Leukodystrophies (LDs) are a group of hereditary diseases affecting the central nervous system (CNS). LDs result in severe and often progressive neurologic disease, primarily affecting young children.[1,2] The possibility of definitive, targeted gene therapies has become a reality for some LDs.[3] One promising target of gene therapy is metachromatic LD (MLD), an autosomal recessive lysosomal storage disease arising from biallelic pathogenic variants in the *ARSA* gene, encoding the enzyme arylsulfatase A (ARSA), which converts 3-O-sulfogalactosylceramide (sulfatide) to galactosylceramide. Decreased ARSA activity disrupts this lipid conversion process, altering the composition of myelin sheaths and inducing a buildup of sulfatides in the CNS and peripheral nervous system (PNS).[1,4] The most common clinical subtype is the late infantile (LI)-MLD form, which results in rapid loss of neurologic skills, beginning before the age of 2.5 years, and early death.[1]

Historically, MLD treatment in the US was based on hematopoietic stem cell transplantation (HSCT),[5,6] which has mixed outcomes especially after symptom onset.[1] Because of the limitations of HSCT, including availability of transplant matches and lack of efficacy in younger children with MLD, an autologous stem cell

Received 12 June 2024; accepted 22 January 2025;
https://doi.org/10.1016/j.omtn.2025.102464.

Correspondence: Stefano Rivella, Department of Pediatrics, Division of Hematology, Children's Hospital of Philadelphia, Philadelphia, PA, USA.
E-mail: rivellas@chop.edu

Published by Elsevier Inc. on behalf of The American Society of Gene and Cell Therapy.
This is an open access article under the CC BY-NC-ND license (http://creativecommons.org/licenses/by-nc-nd/4.0/).

transplant with lentiviral (LV) treatment strategy was developed. The drug product indicated as atidarsagene autotemcel (Lenmeldy in the US or Libmeldy in the European Union [EU]), is made by transduction of autologous hematopoietic stem cells (HSCs) with an LV, indicated in this report as clinical vector (CV), encoding the ARSA gene.[7] CV is approved for treating pre-symptomatic early-onset patients (onset < 7 years) and children, minimally symptomatic, with onset of disease between 2.5 and 7 years old.[8–11] The concept behind the success of the current clinical LV is that supraphysiological expression of ARSA in pre-symptomatic patients via the phosphoglycerate kinase (PGK) promoter provides more enzymatic activity than allogeneic healthy HSCs to suppress the detrimental effects of sulfatide buildup.[8] A key factor in the success of this therapy is the ability of the transplanted bone marrow (BM) product to cross the blood-brain barrier (BBB) and replenish the endogenous microglia.[12,13]

Despite the success of the CV, there is a need to explore whether a more efficient system can be developed given the high vector copy numbers (VCNs) required with the currently available product. This places an increased burden on manufacturing needs and potentially a higher risk of complications such as genotoxicity for the patient. With increasing numbers of viral integration, there is a greater probability of genome toxicity and leukemogenesis, which may place children at increased risk for complications.[14,15] Additionally, while the pre-symptomatic LI-MLD populations respond well to CV, treatment is inadequate to address the needs of early-symptomatic individuals.[1] Additional enzyme activity without increasing the need for integration may be needed to help this population. These limitations suggest that an improved vector design could enhance therapeutic efficacy. To this end, we generated novel vectors to be compared with the CV.

Our vector designs demonstrate greater ARSA expression and activity across biologically relevant cell lines. In addition, our vector allows generation, from the transduced cells, of secreted extracellular vesicles (EVs) loaded with the ARSA protein. *In vitro*, these EVs can transfer the ARSA protein and activity to other cells. Our LVs illustrate a robust safety profile as indicated by genotoxicity assays and transduction into wild-type (WT) mice. Finally, our vector ameliorates MLD disease phenotypes in *Arsa*-KO mice at a lower VCN than the CV. The combination of genetic regulatory elements that increase ARSA expression in our novel vectors can serve as a backbone for other constructs to treat similar lysosomal storage diseases and leukodystrophies, such as multiple sulfatase deficiency (MSD). Developing more efficient vectors is a critical step in reducing genome toxicity and improving outcomes for early-symptomatic patients.

RESULTS

A novel vector design for improved transgenic expression by LVs

Several PGK and elongation factor 1 alpha (EF1α) promoter-driven enhanced green fluorescent protein (eGFP) reporter vectors were designed to assess how ankyrin and foamy insulators and the woodchuck hepatitis virus posttranscriptional regulatory element (WPRE)/bovine growth hormone poly(A) signal (bGHpA, indicated as pA) sequences affected transgene expression (Figure 1A). The *ARSA* gene expression in our LV is driven by the 1.184 kb human EF1α promoter, which demonstrates significantly stronger expression across tissue types compared to other promoters, including PGK.[16,17] The core part of the promoter sequence required for the high level of activity is contained in the 943 bp first intron sequence.[18] In the EF1α promoter, a 231 bp sequence precedes the first intron, comprising the first exon and the 5′ upstream sequence flanking it, which is all a part of the non-coding region. The WPRE (indicated as W) is traditionally utilized to increase viral RNA integrity and titer.[19,20] However, when included in the transgenic cassette (between the 5′ and 3′ long terminal repeats [LTRs]), WPRE limits vector capacity and becomes structurally integrated into the DNA of patient cells. In addition, the human immunodeficiency virus (HIV) polyadenylation signal in the 3′ LTR leaks, allowing viral RNA readthrough.[19] As previously shown,[19] these limitations can be overcome by cloning the WPRE downstream of the 3′ LTR together with the pA. In addition, several laboratories, including ours, have documented the use of insulators to reduce position effects, silencing, and enhance safety.[21–25] We included insulator elements in our LV design, which may minimize undesirable promoter activation and aberrant transcription in regions of LV integration.[18,19]

In the CV, a PGK promoter drives *ARSA* expression, where a mutated WPRE (WPRE6) is downstream of *ARSA* and upstream of the 3′ self-inactivating (SIN) LTR.[9] WPRE6 was generated to prevent potential oncogenic activity of WT WPRE, as described by Kingsman et al.[26] Our constructs were compared to CVG and PGK-G-W vectors, which were identical to CV, except for replacing the *ARSA* transgene with an eGFP reporter gene (Figure 1A) and the non-mutated WPRE sequence in PGK-G-W. PGK-G-W demonstrated the same mean fluorescence index (MFI) as the CVG construct and was used as a comparison to all other vectors in Figure 1. This allowed us to directly compare how the different genomic elements and their rearrangements enhanced transgene expression. We tested these constructs in murine erythroid leukemia (MEL) cells, which are sensitive to integration-based position effects and transgene silencing.[21,27]

The MFI of GFP^+ cells was measured for each vector as a metric of vector potency (Figures 1B, S1A, S1B, and S1C; Table S1). The percentage of transduced positive $eGFP^+$ cells was kept at 10% or below to limit having more than one integration per genome and to assess the MFI in cells predominantly with a single integration (Figures S1A and S1C). The inclusion of the ankyrin insulator (comparing EF1α-W vs. EF1α-W-A) demonstrated a 2-fold increase in MFI (Figure 1B). Rearrangement of WpA (EF1α-WpA) showed an almost 10-fold increase in MFI compared to EF1α-W (Figure 1B). Combining insulators with WpA (EF1α-WpA vs. EF1α-F-WpA, EF1α-A*-WpA, and EF1α-A*F-WpA) had limited effects on the MFI (Figure 1B).

WpA rearrangement significantly increased MFI, which correlated with a ∼2-fold higher eGFP mRNA expression for EF1α-WpA

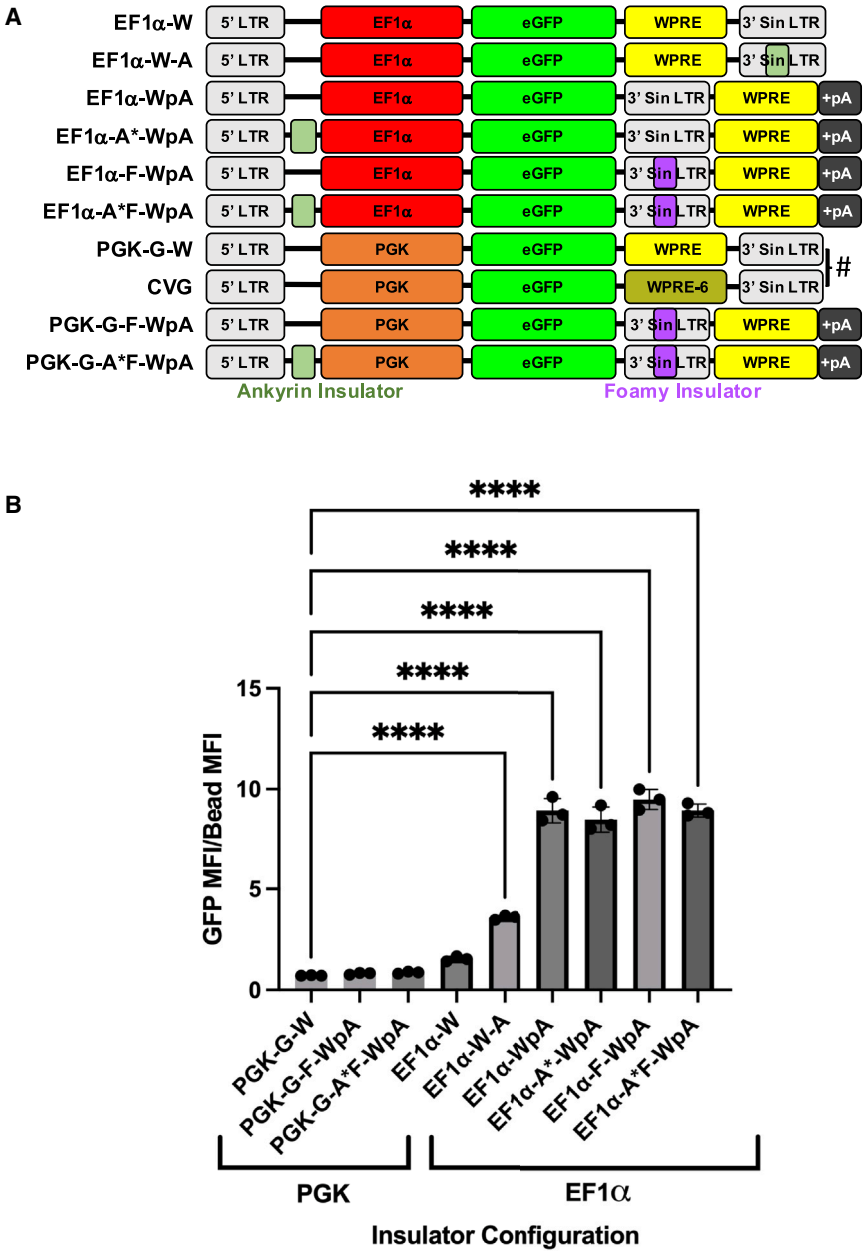

Figure 1. Optimal arrangement of vector components to maximize eGFP expression

(A) Maps of the multiple vector arrangement used to determine the optimal configuration of EF1α promoter with ankyrin or foamy insulators and WPRE (W) with poly(A) tail (pA) region for optimal eGFP MFI. (B) MFI for all EF1α vector arrangements shown above (n = 3) in addition to select PGK arrangement compared to their EF1α counterparts to demonstrate the key expressive benefit of using Ef1α in these arrangements. LTR, long terminal repeat; Sin-LTR, self-inactivating long terminal repeat; WPRE, woodchuck hepatitis virus posttranscriptional regulatory element; WPRE6, mutated WPRE; PGK, phosphoglycerate kinase promoter; EF1α, elongation factor 1a (EF1α) promoter; pA, bovine growth hormone poly(A) signal. ****$p < 0.0001$ Note: significance shown for key comparisons. Expanded significance is shown in Table S1. #PGK-G-W demonstrated the same MFI as the CVG construct and were not statistically different (not shown).

compared to EF1α-W (Figure S2). Overall, the data suggest that removing the WPRE from the 3′ of the eGFP gene promotes mRNA transcription and/or stability and, ultimately, eGFP expression after genomic integration.

Similar modifications were introduced in PGK-based vectors (Figures 1A and S1B). None significantly impacted eGFP expression (Figures 1B, S1B, and S1C with all PGK-driven vector MFI values and statistics described in Figure S1C). However, EF1α-W demonstrated a ∼2-fold increase in MFI compared to PGK-G-W, while EF1α-F-WpA and EF1α-A*F-WpA showed almost a 10-fold increase (Figure 1B). This ultimately led us to use the EF1α-A*F-WpA arrangement of elements to design a more potent *ARSA*-expressing vector compared to the construct of the CV.

Novel LV vectors increase *ARSA* expression and activity in patient-derived fibroblasts and *ARSA*-KO human microglia cells

Based on the preliminary results with the eGFP reporter constructs, we generated six new vectors to drive *ARSA* expression and compared them to an in-house replica of the approved clinical vector for MLD (cloned according to the published literature on atidarsagene autotemcel), indicated as CV (Figure 2A).[11] The ARSA coding sequence was optimized to increase its translation in human cells and/or generate a coding sequence that could discriminate between patient and vector *ARSA* mRNA by RT-PCR (E1–E4). Additional modifications were applied to generate EA1 and EA2, which contained the foamy insulator in the 3′ LTR with and without the ankyrin insulator 5′ of the EF1α promoter. Both vectors contained the sequence-modified ARSA (without UTRs) to retain the ability to discriminate between endogenous and transgenic mRNA sequences, described in Figure 2A.

WT and *ARSA*-deficient primary fibroblasts (cell line 2331) derived from a healthy individual or a patient with MLD, respectively, were used to test ARSA expression and enzymatic activity upon transduction with either CV or one of our vectors. We analyzed ARSA activity, normalized to VCN, in specimens with transduction of VCN 2 or lower to evaluate the correlation between ARSA activity and VCN

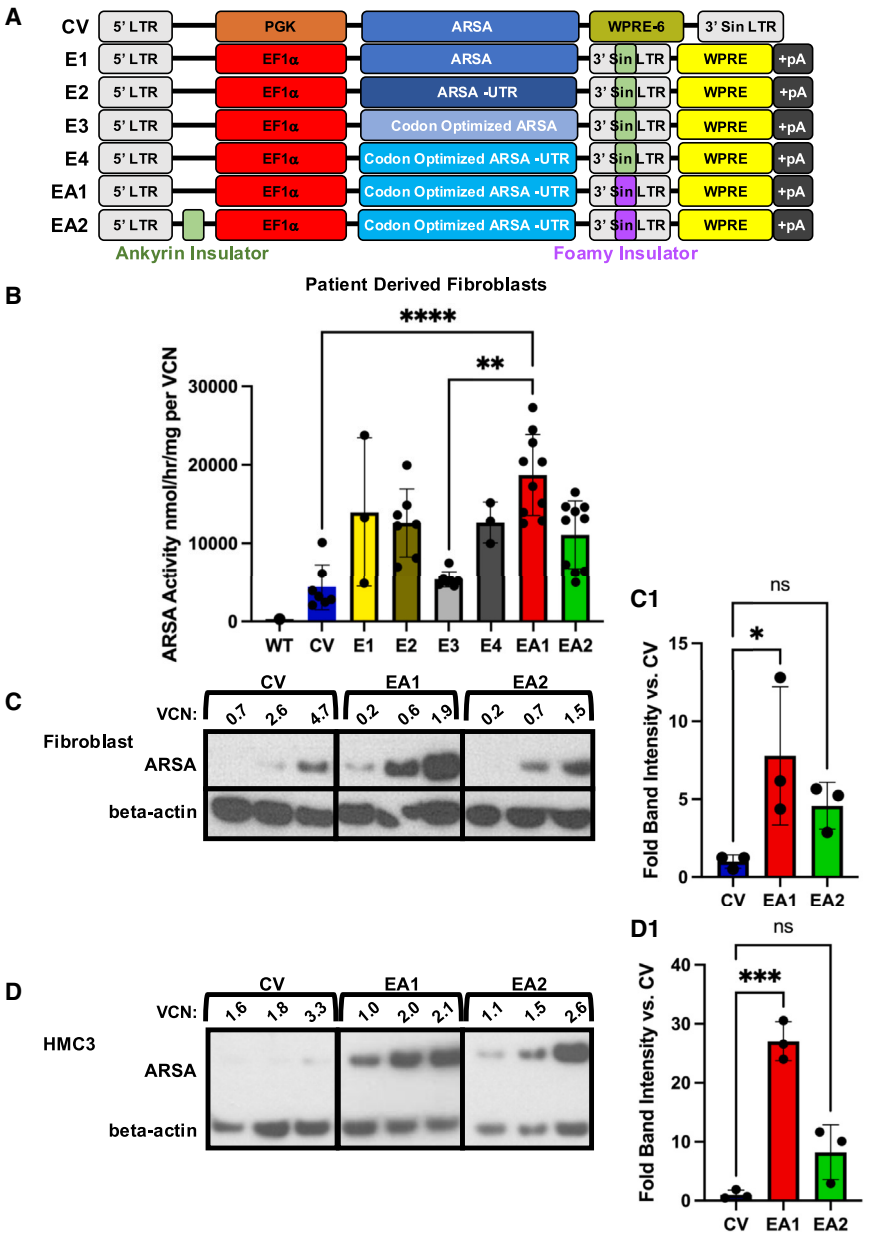

Figure 2. Improved activity and protein expression of ARSA in MLD patient-derived fibroblasts and ARSA-KO human microglia cells

(A) Vector schematics comparing the CV and our six Ef1α vectors used to test ARSA expression based on the best MFIs from the eGFP pilot vectors. (B) Fibroblast ARSA enzyme activity normalized to VCN for our six test vectors, including the CV (n = 3–10). (C) A western blot for ARSA from the same transduced patient-derived fibroblast in (B). (D) A western blot using a human microglia cell line (HMC3-ARSA-KO) transduced with vectors CV, EA1, and EA2. Fold change in band intensity was normalized to beta-actin. (C1 and D1) Quantification of ARSA from western blots shown in (C) and (D) as average from independent experiments; n = 3. LTR, long terminal repeat; Sin-LTR, self-inactivating long terminal repeat; WPRE, woodchuck hepatitis virus posttranscriptional regulatory element; PGK, phosphoglycerate kinase promoter; EF1α, elongation factor 1 alpha (EF1α) promoter. $^{*}p < 0.05$, $^{**}p < 0.01$, $^{***}p < 0.001$, $^{****}p < 0.0001$.

as a linear relationship. CV-treated cells demonstrated enhancement in ARSA activity over WT cell baseline activity (Figure 2B), concordantly with data previously published.[8,9] Comparing E1, E2, E3, and E4 vectors that contained the ankyrin insulator, neither optimization of the coding sequence nor inclusion of the 5′ and 3′ UTRs significantly modified ARSA synthesis. In addition, although we observed a trend in increased ARSA activity in most of these vectors compared to CV, the differences were not significant (Figure 2B). EA1-treated cells showed 4-fold greater activity in ARSA-deficient fibroblasts than those treated with CV (Figure 2B). Therefore, EA1 was chosen for further studies. To assess if the presence of the EF1α intron in the promoter would lead to a significant proportion of viral genomes with a deletion of this region, we analyzed the EA1 viral genomic RNA by next-generation sequencing. The expected full-length sequence was observed in the overwhelming majority of the reads, indicating that most of the genomic RNA preserved the predicted structure, including the WPRE-poly(A) sequence downstream of the 3′ LTR (Figure S3A), as previously seen.[19] We also amplified the sequence of the EA1 vector integrated into mouse BM cells. We observed an intact and full-length PCR product (Figure S3B), corroborating that most, if not all, of the sequences integrated included the EF1α intron. The sequence of the vector EA1, for the LTR to WPRE-pA sequence, and the fully annotated plasmid map are shown in Figures S4 and S5, respectively. At this initial stage of our study, EA2 was also selected because of its structural similarity to EA1 and to test the effect of expressing an intermediate level of ARSA (compared to EA1 and CV). EA1- and EA2-treated fibroblasts demonstrated more transgenic ARSA expression than those treated with CV (Figure 2C). EA1- and EA2-treated specimens synthesized, on average, 7-fold and 4-fold greater ARSA protein (normalized to beta-actin and VCN; expanded description in the materials and methods) than specimens treated with CV (Figures 2C and 2C1). EA1 vs. CV was assessed in transduced human CD34^{+} cells (Figure S6), in which EA1 showed ∼3× more ARSA expression (normalized to VCN) than CV-transduced CD34^{+} cells.

Transfer of ARSA protein to MLD-affected cells in the CNS by HSC-derived microglia may contribute to treatment efficacy through

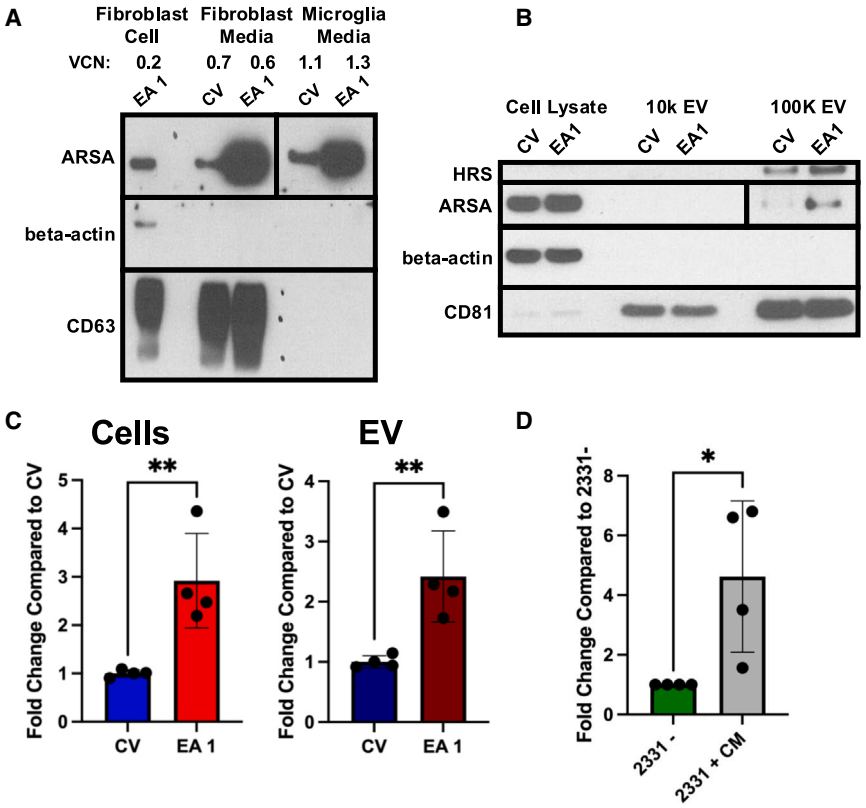

Figure 3. Increased ARSA protein expression and activity in EVs secreted from transduced cell lines

(A) Protein-precipitated medium harvested from vector-transduced patient fibroblasts and *ARSA*-KO microglia cells demonstrated much greater ARSA expression in EA1 than CV by western blot. The VCN of each cell line is noted above the treatment (top left). (B) EVs were then isolated via ultracentrifugation, yielding more expression of EV-related ARSA for EA1 at a VCN of 1.2 compared to CV VCN of 3.5. The cells the medium was derived from (cell lysate) are also shown for comparison in addition to the 10,000 × *g* large-vesicle fraction. (C) Fold change in ARSA activity assay compared to CV for harvested cells and EVs demonstrated higher ARSA activity in cells for EA1 at a VCN range of 0.6–2.4 compared to CV VCN in a range of 3.5–6.8 ($n = 4$). (D) Fold change in ARSA activity of the untransduced patient cell line alone (2331−) compared to when CM is added to the untransduced cells (2331+) demonstrates an increase in ARSA activity to the transferred cell line ($n = 4$). $^{*}p < 0.05$, $^{**}p < 0.01$.

cross-correction but has not been proven to play a role.[28,29] Therefore, ARSA synthesis and activity were also assessed in the *ARSA*-knockout (KO) human microglia cell line (HMC3) exposed to EA1, EA2, or CV. As shown in Figures 2D and 2D1, ARSA expression of EA1- and EA2-treated specimens was, on average, 27-fold and 8-fold greater (again normalized to beta-actin and VCN) than that measured in CV-treated cells (1.8 VCN), further confirming superior ARSA expression over CV.

EV secretion as a modality of ARSA enzyme transfer in the CNS and superior ARSA production by EA1 in EVs

Secreted small EVs ranging from 50 to 200 nm in size have been well demonstrated to transfer functional biological cargo from host to recipient cells. Clinical interest has thus emerged in engineering EVs for the therapeutic delivery of functional enzymes in lysosomal storage disorders, together with other mechanisms of cross-correction.[29,30] Cellular overexpression of target cargo may facilitate physiologic loading and secretion of constitutive EVs from modified cells.

We evaluated secretory levels of ARSA from cell-conditioned medium (CM) of primary patient MLD fibroblasts and *ARSA*-KO microglia after transduction with CV or EA1. EA1-transduced cells demonstrated increased cell-conditioned medium ARSA activity at comparable VCN to CV-transduced cells (Figure 3A). Cell-free CM was depleted of beta-actin and enriched in CD63, a tetraspanin protein associated with secreted EVs.

To measure vesicle-associated ARSA abundance and activity, secreted EVs were isolated from human MLD primary fibroblasts transduced with EA1, EA2, or CV. Levels of ARSA were mainly enriched in small, secreted vesicles isolated after ultracentrifugation (100,000 x g) and enriched in small EV markers Hepatocyte growth factor-regulated tyrosine kinase substrate (HRS) and CD81 compared to larger HRS-CD81^{lo} vesicles isolated after a low-speed (10,000 × *g*) centrifugation (Figure 3B; Figure S7A). Further purification of small EVs using a density-gradient enrichment strategy confirmed that vesicles from EA1- and CV-transduced cells were enriched in ARSA, with detectable levels in EA2-transduced EVs (Figure S7B).[31,32] EA1-transduced cells showed increased ARSA activity in secreted vesicles at lower VCN (EA1 range, 0.6–2.4 versus CV range, 3.5–6.8) (Figure 3C). Functional ARSA activity was enhanced about 2-fold in EA1-transduced cells and secreted vesicles compared to CV-treated cells (Figure 3C). CM from EA1-transduced cells was added to *ARSA*-deficient patient fibroblasts (2331−) to test whether EV-associated ARSA could be functionally transferred. This yielded a significant increase of about 4-fold more cellular enzyme activity compared to the deficient fibroblast cells alone (Figure 3D). These data indicate that EA1 transduction enhances EV-associated secretion of functional ARSA compared to CV. This increased production of the ARSA enzyme will likely impact the enzymatic load delivered to non-hematopoietic cells, which may improve outcomes after gene therapy.

EA1 and EA2 vectors exhibit no observable immortalization in transduced HSCs

In addition to maximizing ARSA expression and activity, vector safety is a vital feature in preclinical consideration. To exclude genome toxicity *in vitro*, we evaluated our vectors' potential to

A

	Wells Transformed	VCN
Control	0/26	0.0
pMSCV-GFP I	0/32	0
pMSCV-GFP II	3/32	1.7
pMSCV-GFP III	11/32	3.1
CV	0/28	4.4
EA1	0/35	6.3
EA2	0/20	4.3
CV	0/48	1.2
EA1	0/43	1.1
EA2	0/40	0.4

B

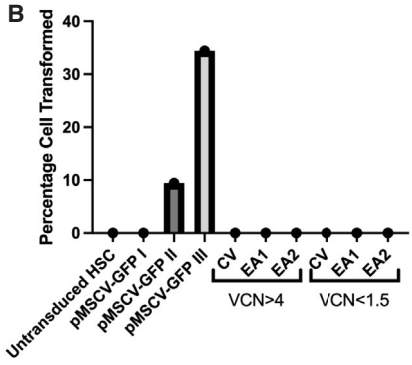

Figure 4. Genotoxicity assay

(A) A table of VCN and percentage of wells transformed in multi-well plate format of vector-transduced mouse HSCs. The positive-control pMSCV-eGFP vector-treated wells are the only plates with cell transformation and medium depletion (yellowing) due to cell immortalization. All other vector-transduced plates after 9 weeks show cellular senescence and absence of medium depletion. (B) A graphical representation of absence in cell transformation in all cell lines aside from the pMSCV-eGFP, indicating the safety of our vector at higher (>4) and clinically relevant (1.5>) VCN.

transform lineage-negative selected mouse BM cells in long-term replating experiments, as shown previously.[33]

Lineage-negative selected mouse HSCs were transduced with CV, EA1, and EA2. LV-transduced mouse HSC cells were compared to mock un-transduced cells, and, as a positive control, we used a well-established gamma retroviral vector named pMSCV-eGFP.[33,34] We did not observe clonal expansion in any of the lentiviral transduced cells, up to 6.4 VCN, while, as expected, pMSCV-eGFP induced clonal expansion starting at week 5 and VCN starting at 1.7 (Figures 4A and 4B). For the pMSCV-eGFP vector, the transformation frequency was proportional to the VCN (Figure 4B).

EA1 and EA2 vectors do not perturb physiological hematopoiesis in transplanted WT mice

We further explored the safety of our vector by transplanting WT mice with eGFP donor marrow alone or transduced with EA1, EA2, and a modified CV vector, where ARSA was replaced by eGFP (CVG from Figure 1A).

Several animals infused with eGFP mouse BM transduced with EA1 and EA2 showed high VCNs (VCN > 5; Figure 5A) analyzed approximately 5 months post HSCT. We did not observe gross abnormalities in erythroid or lymphocyte populations between animals engrafted with transduced or untransduced HSC and WT control mice (Figures 5B and 5C). The percentage distribution of erythroid cells at different stages of maturation (Figure 5B) was similar among cohorts. Lymphoid B and T cell populations demonstrated a comparable percentage distribution in vector-transduced mice compared to controls (Figure 5C, with full flow profiles for every harvested mouse described in Figures S8A and S8B). In addition, the distribution of macrophages between populations was unaltered (Figure 5D). A mouse BM colony-forming unit (CFU) assay showed no difference between treated and control mice (Figure 5E).

Arsa-KO mouse disease model of MLD is corrected with, on average, 5-fold less EA1 vector than CV

We generated a novel *Arsa*-KO mouse model of MLD, as described in Figure S9. This mouse model is expected to recapitulate the phenotype of a previously generated mouse model, which was not available for our studies.[35] In pilot experiments, after 8 months, we observed significant sulfatide accumulation and microglia inflammation in *Arsa*-KO brains, hallmarks of MLD pathology (Figure S10A). However, at 8 months, *Arsa*-KO mice did not demonstrate a significant difference in rotarod performance compared to a control mouse. The motor deficit became apparent in 1-year-old *Arsa*-KO mice, which showed a significant difference on the rotarod, corroborating evidence of disease phenotype and the need to assess mice at 1 year of age (Figure S10B).

With these parameters in mind, we compared the efficacy of therapeutic vectors: 8- to 12-week-old *Arsa*-KO lethally irradiated mice were infused with *Arsa*-KO HSC transduced with CV, EA1, EA2, or control *Arsa*-KO HSCs. Untransduced *Arsa*-KO and WT were used to identify baseline values. Phenotypic rescue was evaluated 10 months post HSCT, at approximately 12 months total age.

Our study aimed to design a vector to prevent MLD disease at lower VCN. Therefore, challenging our vector to outperform CV at lower VCN was critical. Given the potency of EA1 observed *in vitro*, we aimed for a VCN of around 1. On rotarod testing, WT mice (untransduced; age matched) showed improvement in their maximum duration over the course of the 5-day testing period, starting at about 230 s and going to almost 260 s by day 5 (Figure 6A). To assess the performance of the *Arsa*-KO mice after myeloablation, two sets of *Arsa*-KO mice, both age matched, one non-transplanted and the other transplanted with BM from *Arsa*-KO donor mice, were used. Both sets of MLD mice's duration on rotarod were diminished at baseline compared to WT and demonstrated some improvement over the testing period by day 5 (Figure 6A). There were no significant differences in the performance of the transplanted and untransplanted *Arsa*-KO mice. CV-treated mice began at 200 s in duration and improved very little by day 5, generally performing poorly compared to WT (Figure 6A). It is important to note that the 2-VCN range is the clinically relevant VCN for the efficacy of this vector.[7] In contrast, the performance of EA1-treated mice matched that of the WT group, at an average VCN of 0.35 (Figure 6A), about 5-fold less than that of the 1.1–2.6 therapeutic VCN range of CV-treated mice.

As a baseline in the pole-descent assay, WT mice demonstrated significantly more rapid descent times than *Arsa*-KO mice, traversing the pole

A

BM	Weeks Transplanted	VCN
CVG L	23	10.6
CVG N	23	6.7
CVG R	23	6.7
CVG RL	18	8.4
CVG R	18	8.2
CVG RR	18	11.7
EA1 N	23	12
EA1 R	23	2.3
EA1 RR	23	7.3
EA1 L	23	6.2
EA2 RL	23	5.9
EA2 N	23	0.2
EA2 RL	18	0.9
EA2 RR	18	1.9
EA2 LL	18	5.2

*GFP marrow donor transduced to WT recipient

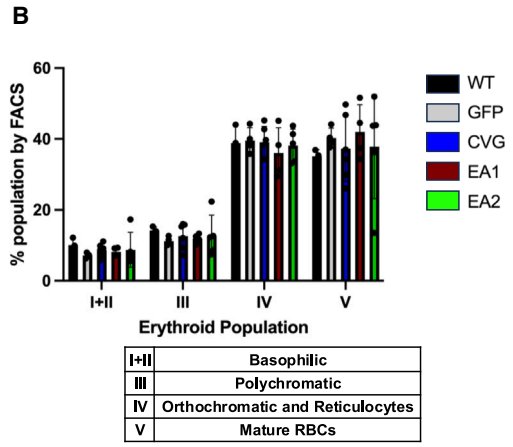

I+II	Basophilic
III	Polychromatic
IV	Orthochromatic and Reticulocytes
V	Mature RBCs

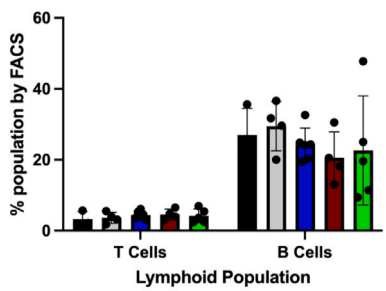

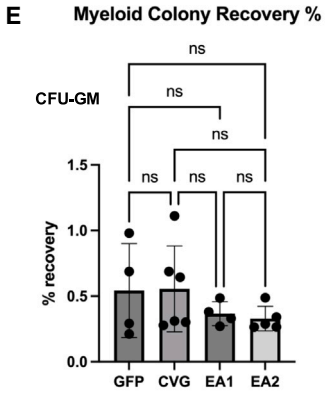

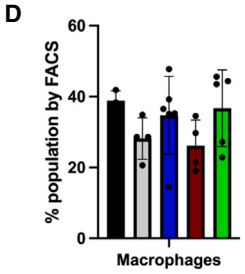

Figure 5. Transduction of eGFP CV, EA1, and EA2 vectors into WT mice demonstrates vector safety

(A) The numbers of weeks post BMT and VCNs are indicated. (B) Erythropoiesis analysis (population I–V, from immature to enucleated red cells) by flow cytometry in WT controls, eGFP mice transduced with normal marrow or mice treated with CVG, EA1, or EA2, from top to bottom. (C) In the same animals, the lymphocyte B and T cell immunoprofiles are shown in addition to (D) the macrophage population. (E) Myeloid progenitor colony formation assay from transduced eGFP mouse mock control, CVG-, EA1-, and EA2-treated mice. CFU-GM, granulocyte-macrophage progenitor.

in about 3 s on average (Figure 6B). WT mice performed with less than half of traction-loss event per trial during descent compared to *Arsa*-KO mice (Figure 6C). In comparison, *Arsa*-KO mice demonstrated the longest descent times, averaging around 7 s, and significant difficulty gripping the pole, with an average of over one traction-loss event per trial during the descent (Figures 6B and 6C). CV-treated *Arsa*-KO mice had an average descent time of over 4 s and significantly differed from untreated *Arsa*-KO mice. However, the overall traction-loss events for all CV-treated cohorts were similar, showing no significant difference to *Arsa*-KO mice, again highlighting a lack of complete disease prevention for CV irrespective of VCN. The EA1 cohorts showed more significance than CV compared to *Arsa*-KO for descent times, with an average descent of 3.8 s. Traction control on the pole during the EA1 group's descent was in line with WT mice. The marked improvement in motor function with EA1 treatment was accomplished with an average of only 0.35 VCN of vector integration across all VCN-treated groups compared to 1.1–2.6 VCN for the CV cohort with a higher VCN. These data consolidated EA1 as our best vector and highlighted the 5-fold increase in vector potency, which aligns with the *in vitro* results. The chimerism in transplanted mice was above 80% and comparable among experimental groups (Figure 6D). Secondary transplants were performed from primary transduced EA1 mouse whole BMs, and no gross abnormalities in hematopoiesis were demonstrated by flow cytometry (Figure S11).

Histopathology demonstrates correction of MLD phenotype in line with behavioral analysis

To determine if lower VCN in treated EA1 mice with improved behavior is accompanied by amelioration of brain physiology, we performed neuropathology on the brain sections of the same treated mice at 12 months of age. *Arsa*-KO mice presented many sulfatide bodies in the corpus callosum and other brain areas relative to WT mice (Figure 7A). Quantification of sulfatide bodies indicated that EA1-treated mice dosed with lower VCN (at 0.6) had counts in line with WT mice. In the CV cohort with lower VCN (0.6), sulfatide bodies demonstrated more accumulation compared to that of the EA1 cohort (Figures 7A and 7A1). The CV cohort with higher VCN showed no sulfatide bodies and efficiently corrected this phenotype (Figure S12A; Table S2).

Next, we evaluated myelin deficits and patterns using eriochrome cyanine (Eri-C) staining in *Arsa*-KO mice. *Arsa*-KO mice demonstrated demyelination spots or vacuoles (Figure 7B, indicated by white arrows) compared to WT mice. We quantified these demyelination vacuoles in untreated and treated groups (Figure 7B1). Mice treated with EA1 at VCN of 0.6 showed no vacuoles and well-preserved myelin. In comparison, mice treated with CV at lower VCN failed to show complete correction in myelin. Only at VCN > 1.1 did CV-treated mice show improving phenotypic features (Figures 7B1 and S12B; Table S3).

Further, to evaluate neuroinflammation in *Arsa*-KO mice, we performed GFAP and Iba1 staining in astrocytes and microglia.

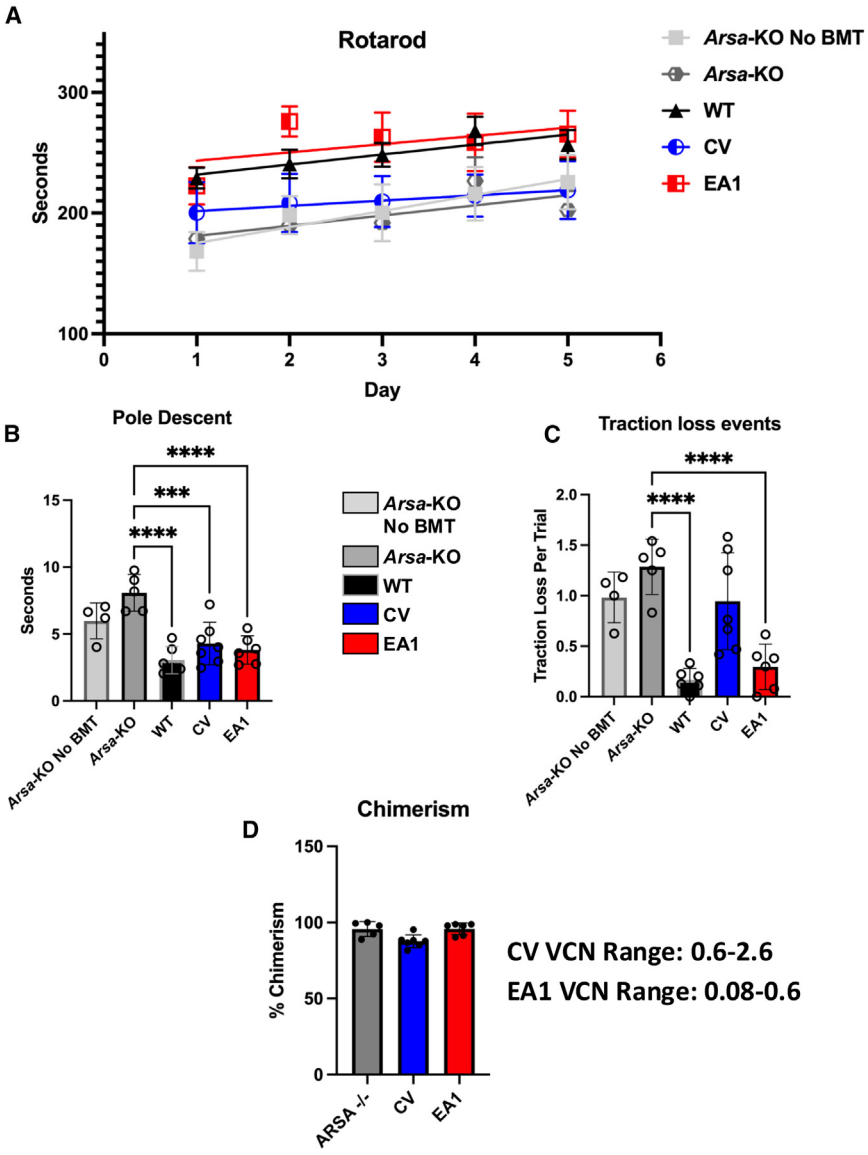

Figure 6. Rotarod and pole descent motor control assays of untreated *Arsa*-KO disease mice compared to vector-treated mice

(A) Rotarod assessment over a 5-day time course for WT, untreated, or CV or EA1 vector-treated mice (n = 4–7). (B) Descent time duration for a predetermined pole segment in vector-treated groups compared to *Arsa*-KO mice (n = 4–7). (C) Report of times mice slipped or lost grip during the pole-descent assay (n = 4–7). (D) Table of mice assessed and corresponding VCN and chimerism. ***$p < 0.001$, ****$p < 0.0001$.

Arsa-KO mice showed increased astrogliosis and microgliosis relative to WT mice (Figures 7C and 7D). In the treated groups, EA1-treated mice at lower VCN (0.6) exhibited no neuroinflammation in different areas; instead, CV-treated mice with equivalent VCNs demonstrated some astrogliosis and microgliosis (Figures 7C1 and 7D1). At higher VCNs, CV-treated mice demonstrated complete correction (Figures S12C and S12D; Tables S4 and S5).

Overall, our novel EA1 vector is highly efficacious in ameliorating the disease phenotype at considerably lower VCN.

DISCUSSION

We have engineered a novel LV for autologous hemopoietic stem cell gene therapy of MLD that provides more robust ARSA expression at lower VCN compared to a copy of the clinical vector currently approved in the US and EU for MLD, here named CV. *In vitro*, the EA1 vector produces 4× more ARSA activity per VCN than CV. This prevented the development of the MLD phenotype in *Arsa*-KO mice with, on average, 5× fewer copies per genome (VCN 0.35) of EA1 than CV at clinically relevant therapeutic range (VCN 2). In previous experiments with a vector-like CV, a protective effect in *Arsa*-KO mice was achieved with VCN in the range of 3–9.[8] In patients, a vector-like CV produces a protective effect closer to the 2-VCN range.[7,9] This highlights the need for a more robust vector to accomplish the same effect at a much lower VCN. The low VCN in MLD animals rescued by EA1 could limit possible genotoxic effects and improve manufacturing efficiencies, improving equity and access. There is also the potential that a more efficient vector could require less myeloablation, further reducing potential therapy-related complications. With the adrenoleukodystrophy lentiviral product, the risk of myelodysplastic syndrome highlights the need to develop safer gene therapy vectors.[36] We have taken further precautions by including insulator elements to help mitigate insertional genotoxicity.[23,24,37] Achieving the most optimal expression possible while maintaining safety should be the benchmark for new cutting-edge gene therapies.

In our hands, EA1 transduces human CD34$^+$ cells very efficiently, with a minimal MOI of 10, which yielded a VCN of 1.8. In transplanted mice, EA1 VCNs in the range of 1 were achieved with low MOI. Given the current hurdles and costs in LV production, our vector provides a strong case for being less expensive (reduced MOI to achieve optimal transduction), and efficient (low VCN to be effective).[38] Compared to CV, if a lesser amount of vector can be implemented to achieve the same effect, this could drastically reduce the cost of vector production. Atidarsagene autotemcel is one of the most expensive therapies, priced at $4.25 million

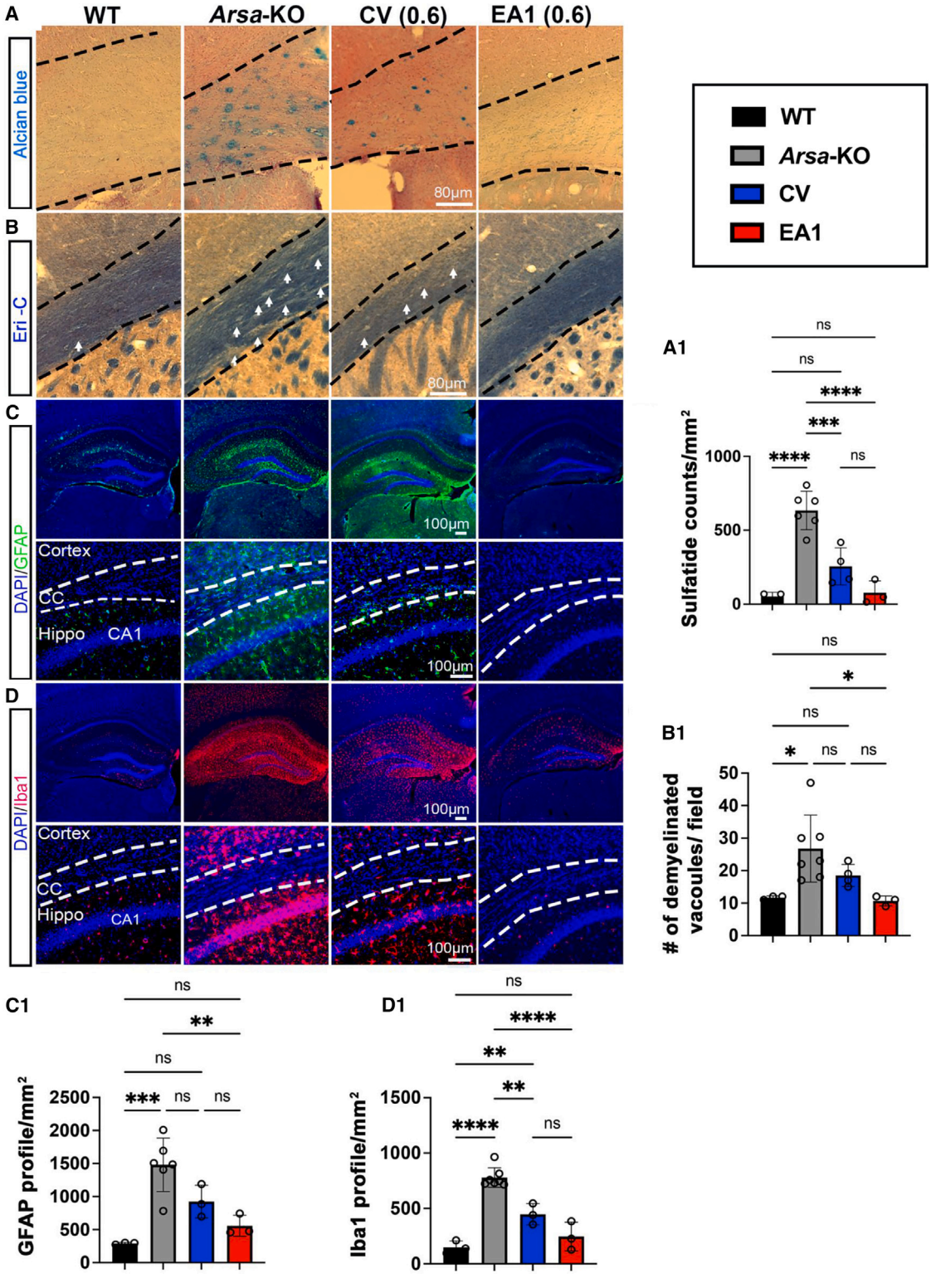

(legend on next page)

or €3 million per treatment.[39] The high cost of existing gene therapies poses a significant challenge to delivering transformative treatments to patients. Although the current gene vector is effective for a subset of children with MLD, there remains a critical need for more efficient, cost-effective approaches. These advancements would expand accessibility, enabling broader patient populations to benefit from potentially life-saving therapies while reducing the financial burden on healthcare systems. Given that LV treatments are becoming increasingly mainstream as a highly effective treatment strategy, we must strongly consider making our vectors more competitive for widespread and affordable implementation.[40] The amount of CV integration required for effective treatment is a critical consideration for viable treatment of MLD. For the first time, we have demonstrated that the CV has a limited effective range in protective ability to prevent MLD in an *Arsa*-KO mouse model. Mice treated at around and below 1 (at low) VCN showed no amelioration in behavior on rotarod analysis, pole descent, and traction-loss events and performed similarly to the untreated *Arsa*-KO mice overall.

Cross-correction and transfer of functional ARSA enzyme from microglia to the surrounding CNS is a potential treatment modality, although this is controversial.[28,29] We determined EVs to be a significant source of ARSA secretion. *In vitro*, conditioned medium containing EVs served as a source of active ARSA enzyme transfer from transduced cells to untransduced ones, with EA1 producing more functional ARSA per VCN in EVs than CV. As ARSA-deficient CNS neurons are not directly corrected during MLD gene therapy, effective treatment relies upon optimal secretion of the enzyme from BM-derived microglia that repopulate the nervous system.[12] Since there is only one opportunity per patient for the adoptive transfer of autologous gene-modified cells, the amount of ARSA secreted from microglia, including into EVs, should be maximized for delivery into other CNS cells.

As we advance therapy development across the leukodystrophies (and rare diseases in general), we face serious limitations regarding vector production and concerns about increased risk with increased copy requirements. We propose that a more efficient vector system, such as EA1, may meet the growing needs of the rare-disease community. This has the potential to also support populations that are not currently served by commercial vectors, including symptomatic and late-onset populations. Currently, the existing atidarsagene autotemcel is approved only for pre-symptomatic and early-symptomatic patients. This, in turn, requires neonatal/prenatal screening or a familial history of MLD to address this population of children. However, widespread identification of the broad panel of rare diseases, such as MLD and other lysosomal storage disorders, is still lagging.[41,42] Therefore, being adequately prepared to overcome diseases at any stage is critical for successful treatment. With our more potent EA1 vector, we may be able to offer options for children of families currently with no alternative and address a population over a much broader range of clinical manifestations.

The effectiveness of the improved backbone and regulatory elements in LV design[1,41,42] has a potential to make an impact on other related leukodystrophies, such as MSD. The ability to address multiple associated diseases with a single vector backbone highlights the versatility and advancement of our lentiviral vector program.

MATERIALS AND METHODS

Cell lines

MLD patient fibroblast cell line, designated GM02331, was generated by Adeline Vanderver (Children's Hospital of Philadelphia [CHOP] IRB 14-011236) and maintained in MEM supplemented with 15% non-heat-inactivated fetal bovine serum (FBS) with 10% penicillin/streptomycin (pen-strep). *ARSA*-KO microglia cell lines were generated using human HMC3 cells. CRISPR was utilized by Synthego to develop *ARSA*-KO cells according to the strategy outline in Table S6. Cells were then cultured according to ATCC guidelines, and single cells were sorted to derive a homogeneous population of characterized HMC3 *ARSA*-KO cells. Colonies were expanded and sequenced to verify the KO of ARSA and the lack of ARSA synthesis. One of these colonies was selected as our model microglia *ARSA*-KO line and indicated as HMC3 14.

$CD34^+$ cells were thawed by rapidly incubating them at 37°C and then adding a 10× volume of IMDM 5% FBS drop by drop. Cells were first prestimulated in StemSpan serum free expansion medium (SFEM) (09650, STEMCELL Technologies, 1618 Station Street Vancouver, BC, V6A 1B6, Canada) supplemented with 300 ng/mL hSCF (300-07, PEPRO TECH, 29 Margravine Road London W6 8LL, UK), 300 ng/mL hFLT3 (300-19, PEPRO TECH), and 100 ng/mL hTPO (300-18, PEPRO TECH). Cells were transduced with 10 MOI of EA1 two times, 12 h apart, using Poloxamer 338 2 μL/mL (P2164021, Sigma) and PGE2 0.141 μL/mL (72192, STEMCELL Technologies) as adjuvants. Cells were then subsequently cultured for 2 weeks in expansion medium (StemSpan SFEM supplemented with CC-100 10 μL/mL; 02690,STEMCELL Technologies), Epogen (55513-126-10, Amgen, Thousand Oaks, CA) 1 μL/mL, dexamethasone 1 μL/mL (D2915, Sigma Aldrich), and pen-strep 10 μL/mL(15140-122, LifeTechnologies, Carlsbad, CA) before harvest for ARSA activity assay.

Figure 7. Neuropathological deficits of untreated *Arsa*-KO diseased mice relative to vector-treated mice

Treatment groups include WT, untreated, CV, and EA1 vector treated at lower VCN. (A) Representative images of sulfatide accumulation in the corpus callosum across treatment groups. (A1) Quantification of sulfatide accumulation across groups. (B) Representative myelin staining (Eri-C) images of the corpus callosum in treatment groups. (B1) Graphical presentation of # of demyelinated vacuoles as shown by white arrows in (B). (C) Representative immunofluorescent images of GFAP (astrocytes) in different brain areas. (C1) Astrocytes (GFAP) counts/mm^2 in the corpus callosum. (D) Representative immunofluorescent images of Iba1 (microglia) in different brain areas. (D1) Microglia (Iba1) counts/mm^2 in the corpus callosum (n = 3–6 per group). *$p < 0.05$, **$p < 0.01$, ***$p < 0.001$, ****$p < 0.0001$. Extended significance is shown in Tables S2–S5.

Plasmid, virus production, and transduction of MEL cells

We used PGK or EF1α promoters to drive transcription of the gene encoding the eGFP to assess more robust vector constructs. Vectors were constructed with an eGFP reporter to determine the MFI.[22] LV constructs were designed in our laboratory, and all plasmids were manufactured by Genscript (Piscataway, NJ). Plasmid DNAs were expanded and isolated using a Qiagen Maxiprep kit (catalog no. 12162, Germantown, MD).

Our LV vectors were assembled using a third-generation LV system (VSVG, REV, and RRE) in 293T cells and concentrated via ultracentrifugation.[19] eGFP vector construct transductions were conducted in MEL cells.[21] MEL cells are erythroid progenitors derived from isolation of Friend virus-infected spleen cells of Swiss mice, and their development is arrested at the proerythroblast stage.[43] MEL cells were isolated by and distributed from the laboratory of Drs. Marks and Rifkind at Columbia University, New York.[43] MEL cells were grown in RPMI (Cellgro, Corning, Glendale, AZ) and supplemented with 10% FBS (Hyclone, South Logan, UT) and 1% pen-strep. Transduction was conducted at 5×10^5 cells/mL concentration, complemented with 1% polybrene (Millipore, Billerica, MA).

MEL cell erythroid differentiation was achieved by seeding 2×10^6 cells, in log phase, into 3 mL of fresh culture medium containing N,N′-hexamethylene bis(acetamide) (HMBA) at a final concentration of 1 mg/mL. Treatment with HMBA (Millipore Sigma, Burlington, MA) was repeated after 2 and 4 days of culture, with cells being collected for analysis after 7 days. MEL cells were transduced with a low titer of virus and were assessed to have under 20% eGFP% by flow (Figure S1A). This was essential to ensure MFI was proportional to one integration per cell (under 20% eGFP+). BD FACSCanto (Piscataway, NJ) was used for flow cytometry analysis.

ARSA activity assay

ARSA activity was assessed through a nitrocatechol colorimetric sulfatide assay.[44] ARSA activity was measured in nmol/h/mg. ARSA colorimetric activity assay was conducted as outlined by Baum et al.[44] Assay details were taught by David Wenger from Thomas Jefferson University and adopted to a 96-well plate by us. Briefly, frozen pellets were sonicated at 50% amplitude in 1 s pulse on and 1 s off for six pulses. 4-Nitrocatechol substrate, phosphate reaction buffers, and NaOH solutions were all prepared as outlined by Baum et al.[44] After reaction quenching, 300 μL of the liberated nitrocatechol reaction volume was added to a well of a 96-well plate, and absorbance was read at 515 nm.

ddPCR

Primers for PSI (HEX, Bio-Rad custom assay, Hercules, CA) were used to detect viral integration and PCBP2 (FAM, Bio-Rad custom assay) as an integrated control in mouse cells and RPP30 (FAM, Bio-Rad custom assay, Hercules, CA) in the human fibroblast cells. Reactions were done with ddPCR Supermix for probes (no dUTP) (Bio-Rad, Hercules, CA). Primers are detailed in Table S7 ddPCR plates were prepared using a Bio-Rad automated droplet generator and Px1 plate sealer. The PCR was conducted on a Bio-Rad C1000 thermocycler and analyzed on the Bio-Rad QX200.

Acetone precipitation and conditioned-medium transfer

We conducted a TCA-DOC culture-medium protein precipitation according to Pare et al.[45] to assess for medium secretion of ARSA. After 72 h of culture, acetone precipitation was conducted on medium harvested from these cells to precipitate all secreted proteins. The concentrated medium preparation was run on a western blot and probed for ARSA.

Conditioned medium was generated by incubating EA1-transduced fibroblasts in growth medium for 72 h. The conditioned medium was centrifuged at 300 × *g* for 5 min to precipitate any left-over cells or cellular debris. The supernatant was harvested for ARSA activity assay or incubated with untransduced fibroblasts for 48 h. Harvested conditioned medium was concentrated using a Centricon plus centrifugal filter for 100 kDa before measuring activity. Conditioned-medium-incubated fibroblasts were then phosphate-buffered saline (PBS) washed 2× after medium incubation, then cell pellets were harvested and lysed for ARSA activity levels as described by the ARSA activity assay.

EV enrichment and purification

EVs from transduced fibroblast cultures were harvested using the previously described ExtraPEG method.[46] Briefly, cell-conditioned medium was centrifuged at 500 × *g* for 5 min, 2,000 × *g* for 10 min, and then 10,000 × *g* for 30 min before incubating with a 1:1 volume of 2× PEG solution (16%, w/v, polyethylene glycol, 1 M NaCl) overnight. Solutions were centrifuged for 1 h at 100,000 × *g* to obtain crude EV pellets. Pellets from 10,000 × *g* and 100,000 × *g* spins were lysed in 2× nonreducing Laemmli sample buffer (4% SDS, 100 mM Tris-HCl [pH 6.8], 0.4 mg/mL bromophenol blue, 20% glycerol) for immunoblot analysis. For further purification of small EVs, pellets from 100,000 × *g* spins were resuspended in 1.5 mL of 0.25 M sucrose buffer (10 mM Tris, pH 7.4) for bottom-loaded flotation gradient separation. Briefly, 60% iodixanol (Optiprep; Sigma, D1556, St. Louis, MO) was added 1:1 to the EV/buffer solution and transferred to the bottom of a 5.5-mL ultracentrifugation tube. Subsequently, 1.3 mL of 20% iodixanol and 1.2 mL of 10% iodixanol were carefully layered on top. Gradients were ultracentrifuged at maximum speed in an SW-55 rotor for 70 min with minimum deceleration break. Ten fractions of 490 μL were taken from the top of the gradient. Fractions 3, 5, and 6, previously demonstrated to contain purified EVs,[31,47] were diluted in PBS and washed by ultracentrifugation at 100,000 × *g* for 2 h before lysis in 2× nonreducing Laemmli sample buffer for immunoblot analysis. We have previously published extensive and reproducible characterization of purified vesicles following these detailed approaches according to minimal information for studies of EVs (MISEV) 2018 guidelines.[31,32,46,48]

Long-term replating assay

Transduction of HSCs was performed to achieve VCNs in the range of 4–6 to maximize transformation. Following 2–3 weeks of

expansion post transduction to achieve millions of cells for replating, cells were plated into multi-well culture dishes and replated as the proliferation of the cells dictated. Transformed cells grow and consume medium, while cells in which genomic mutagenesis did not occur enter senescence and stop growing. Mouse HSC cells were transduced with a pMSCV-eGFP vector as a positive control of cell transformation. In contrast, cells transduced with EA1, EA2, and CV demonstrated no immortalization of mouse HSCs after 9 weeks in culture. This was indicated by a lack of medium depletion (and confirmed by microscopy) with VCN ranging from 1.0 to 6.3.

CFU assay

Whole BM cells were isolated from WT-transduced and WT-untransduced harvested mouse bones. Whole BM cells were suspended in MethoCult GF M3534 (StemCell Technologies, Vancouver, Canada) as indicated by the manufacturer. Briefly, cells were resuspended in a 3-mL thawed aliquot of MethoCult GF M3534. After preparation in the 3-mL syringe with the 16-gauge blunt-end needles (28110), 1.1 mL of cells was dispensed per well into a 6-well SmartDish to a final concentration of 50,000 cells per assay well. The myeloid population was interesting for CFU assay because it is the progenitor population crossing the BBB after BMT to generate microglia. Each condition was plated in duplicate according to the MethoCult technical guide. The assay measures the number of colonies formed in the myeloid-defined medium after 2 weeks in culture using the stem vision plate analyzer (Stem Cell Vision, Stem Cell Technologies, Vancouver, Canada).

Mice, lineage-negative selection, and mouse BM transplantation

Arsa-KO (Cyagen, Santa Clara, CA). eGFP or WT were purchased from the Jackson Laboratory (Bar Harbor, ME, USA) CD45.2 mice were bred at the CHOP facility. Lin^- cells isolated from the BM of donor mice (8–12 weeks old) via immunomagnetic separation using a mouse lineage cell depletion kit (Miltenyi Biotec, Auburn, CA, USA). Lin^- cells were transduced overnight at a viral multiplicity of infection (MOI) of 0.3–50 (Table S8) in StemSpan SFEM culture medium (StemCell Technologies, Vancouver, Canada) supplemented with 50 ng/mL recombinant murine stem cell factor (SCF), 10 ng/mL recombinant murine interleukin (IL)-6, 6 ng/mL IL-3 (PeproTech, Rocky Hill, NJ, USA), 200 mM L-glutamine, 100 U/mL pen-strep (Gibco, Thermo Fisher Scientific, Waltham, MA), and 2 μL of Lentiblast Premium (OZBiosciences, San Diego, CA). Specific cell numbers and MOI for CV, EA1, and EA2 Arsa-KO mouse transplants are found in Table S8. A minimum of 300,000 viable Lin^- donor cells in PBS (Gibco, Thermo Fisher Scientific, Waltham, MA) were intravenously injected into lethally irradiated ARSA-KO recipient mice (8–12 weeks old) of the opposite gender. For WT mice, two rounds of virus transduction were performed 18 h apart at MOI between ∼10 and 50.

Behavior assays

Rotarod assays were started with a training period 2 days before the assay time. Mice were trained at 10 rpm for 300 s. Mice were placed back on the rod if a fall occurred to acclimatize them. Three trials were done with a 15-min break between each trial. The trial began 2 days after the training period and was conducted with a 5- to 40-rpm ramp over 300 s. This was done for three trials with a 15-min break between 5 days in a row. Pole-descent assay was conducted using a ring-stand rod taped and covered with a cloth lab sheet for grip. The top was covered with a large spherical object to prevent mice from going to the top and hugging the pole. The tape was placed as a starting region for the first 5–6 cm. The distance from the tape start to the bottom was approximately 34 cm. An acclimation period was conducted for the mice to familiarize them with the space and rod until a basic proficiency for descent was reached. All animals were video recorded during descent; times and loss of footing/traction were assessed from the recording after passing the marked tape start line. The pole-descent assay metrics were split into two parameters: time of descent over a specified pole distance and loss of traction events for the mice during descent. A traction-loss event was defined as a sudden and uncontrolled fall, drop, or slip downward during pole descent, reported as events per trail. Descent time was evaluated by measuring the uninterrupted downward movement of the mice across half of a section of the 34 cm traversed (approximately 17 cm). Change of direction, upward movement, or stopping on the pole was not part of the descent-duration measure. This ensured the highest fidelity and robustness of measured descent data, accumulating more measures of descent time per trial and eliminating aberrant/uncontrolled movement and variability from assessed times.

Western blot analysis

Protein was quantified with Pierce BCA Protein Assay Kit (Thermo Fischer Scientific, Waltham, MA). Gels were run on a NuPAGE 4%–12% Bis-Tris 1.5 mm × 12-well gel (Thermo Fischer Scientific, Waltham, MA). The transfer was conducted onto a polyvinylidene fluoride (PVDF) membrane (Bio-Rad, Hercules, CA). Gels were probed with antibodies against hARSA (R&D systems, Minneapolis, MN), CD63 (Abcam, Waltham, MA) beta-actin (Santa Cruz, Dallas, TX), HRS (Santa Cruz, Dallas, TX), calnexin (Santa Cruz, Dallas, TX), Rab5 (Abcam, Waltham, MA), Syntenin-1 (Abcam, Waltham, MA) CD81 (Santa Cruz, Dallas, TX), and CD9 (Millipore, Darmstadt, Germany), then visualized with SuperSignal Extended Duration Substrate (Thermo Fischer Scientific, Waltham, MA). Audioradiography films (Thomas Scientific, 1141J52, Swedesboro, NJ) and band densitometry were analyzed by ImageJ (https://imagej.net/ij/index.html). Beta-actin band intensities were normalized internally to the lowest beta-actin signal for each vector-treated sample VCN series. Human ARSA band intensity was then normalized to beta-actin for each lane. Finally, each beta-actin-normalized ARSA band intensity was normalized to its respective VCN. These normalized values were then used to determine the fold change in band intensity compared to the CV. All raw audioradiograms are presented in Figures S13–S18.

Flow cytometry

Flow cytometry was performed using a BD FACSCalibur (BD Biosciences, Franklin Lakes, NJ) instrument. Erythroid populations were characterized using fluorescein isothiocyanate (FITC) anti-mouse CD71 (113806) and APC Anti-Mouse Ter119 (116212), PE

anti-human/mouse CD44 (103008), as well as 7-AAD Viability Staining Solution (420404) (Biolegend, San Diego, CA). Lymphoid populations were characterized using APC anti-mouse CD3 (100236, Biolegend, San Diego, CA) and PE-Cyanine7 CD45R (B220) monoclonal antibody (RA3-6B2) (25045282, Thermo Fisher Scientific, Waltham, MA). The flow cytometry results were analyzed using FlowJo v10.8 Software (BD Life Sciences).

Histological processing

Mice were anesthetized and transcardially perfused with an initial flush of PBS followed by 4% paraformaldehyde (PFA). Anesthetic was provided by weight-based injection of a mixture of ketamine/xylazine for adult mice (>P21) with a supplemental isoflurane/oxygen flow. The harvested whole-brain tissue was post-fixed with 4% PFA in PBS overnight at 4°C, then rinsed in 1× PBS (Thermo Scientific) and transferred to 30% sucrose in PBS at 4°C until the sample was no longer buoyant (>3 days), indicating penetrance of the sucrose solution. The whole brain was then embedded in a Tissue-Tek Optimum Cutting Temperature compound (Sakura, 4583) and cryosectioned by a cryostat microtome (Leica, CM3050S) into 50-µm sections in a coronal orientation. Sections were stored in free-floating in PBS and transferred to a freezing medium composed of a mixture of DMEM containing HEPES (Gibco 11885084 and Sigma H7523, respectively) and glycerol (Sigma G6279-500) for long-term storage at −20°C.

Staining

Alcian blue solution was prepared using 3% glacial acetic acid (Amresco, 0714-500) and Alcian blue 8GX (Sigma, A-5268) with a pH adjusted to 2.5 and filtration after overnight stirring. Brain sections of thickness 50 µm were mounted onto a Superfrost Plus slide glass (Fisher, 12-550-15) and dried at room temperature. These slides were then quickly hydrated in distilled water, submerged in 3% acetic acid, and incubated in Alcian blue solution for 1 h at room temperature. Sections were washed in tap water and rinsed in distilled water before exposure to Nuclear Fast Red Counterstain (Vector, H-3403). After washing in tap water, slides were dehydrated in increasing ethanol gradients, cleared with Histo-Clear (National Diagnostics, HS-200), and cover-slipped with Thermo Fisher Gold Seal Cover Glass 24 × 60 mm no.1 thickness (Electron Microscopy Sciences, 63770-01). Sections were imaged using a Leica CTR6000/B microscope to quantify sulfatide accumulation in different brain areas.

Eriochrome cyanine (Eri-C) staining was conducted using previously established methods.[49] Sections were imaged using a Leica CTR6000/B microscope, and ImageJ software was used to quantify demyelination vacuoles in the corpus callosum.

For immunofluorescence, brain sections of thickness 50 µm were washed in PBS, blocked in 10% normal goat serum (EMD Millipore, S26), 2% bovine serum albumin (Sigma, A7030-100G), and 0.1% Triton X-100 (Sigma, T-9284) in PBS for 1 h at room temperature and incubated in primary antibodies (Anti-GFAP, DDRC hybridoma, courtesy Dr. Judith Grinspan, IHC dilution 1:1; Anti-Iba1, FUJIFILM Wako Pure Chemical Corporation, 019-19741, IHC dilution 1:250; anti-NeuN, Millipore Sigma, MAB377, IHC dilution 1:250) overnight at 4°C. Following this incubation, sections were washed with 0.1% Triton X-100 (Sigma, T-9284) in PBS, incubated in fluorescent secondary antibodies for 1 h, and protected from light at room temperature. The secondary antibodies used in this study are Alexa Fluor 488, Alexa Fluor 555, and Alexa Fluor 647 conjugated secondary antibodies against rat (Invitrogen, A21208), mouse (Invitrogen, A315570), and rabbit (Invitrogen, A21245) at 1:1,000 dilutions. Sections were sequentially washed with 0.1% Triton X-100 (Sigma, T-9284) in PBS, counterstained with DAPI, and mounted onto Superfrost Plus Microscope Slides (Fisher, 12-550-15). The tissues were mounted using ProLong Gold Antifade Mountant with DAPI (Thermo Fisher, P36931). Sections were imaged using a Keyence BZ-X810 microscope and a Keyence BZ-X800 Analyzer system to quantify the immunofluorescence staining.

Statistics

All statistical analysis was performed using Prism 10 for MacOS (GraphPad Software, Boston, MA, USA, www.graphpad.com, San Diego, USA). A comparison of two independent groups was conducted by unpaired t test (Figures 3C and 3D). A normality and lognormality test was done on all data at an alpha of 0.05. Depending on the normality of data, either a one-way ANOVA or a nonparametric analysis was applied to compare more than two groups. In Figure 1B a Holm-Šídák's multiple comparisons test was done. For Figures 2C1, 2D1, 6B, and 6C a Dunnett's multiple comparisons test was done. In Figures 5E, 7A1, 7B1, 7C1, and 7D1, a Tukey's multiple comparisons test was completed. In Figure 2B, a non-normal distribution of data and a nonparametric analysis with a Kruskal-Wallis test and Dunn's multiple comparison test was conducted. Rotarod data are presented as SEM. The rest of the data are represented as mean ± standard deviation. Significance levels were $*p < 0.05$, $**p < 0.01$, $***p < 0.001$, and $****p < 0.0001$. If no statistical significance was found, it was not reported.

DATA AVAILABILITY

All BM transplantation studies in mice were approved by the IACUC (protocol #1173) at the CHOP. Reporting of animal studies has been provided per ARRIVE guidelines. Additional data supporting this study's findings are available on request from the corresponding author. No public repository data have been generated for this publication.

ACKNOWLEDGMENTS

David Wenger from Thomas Jefferson University was instrumental in training us on the ARSA colorimetric enzymatic assay, allowing us to adapt it for our laboratory use in 96-well-plate format. Support was received from the Digestive and Kidney Diseases Institute of the National Institutes of Health (R01 DK133475 and R01 DK095112), Institute for Translational Medicine and Therapeutics (ITMAT), Irish Health Research Board-Health Research Charities Ireland (HRCI-HRB), Acceleration-Seed program/CHOP, and The Sickle Cell and Red Cell Disorders Curative Therapy Center (CuRED)-Frontier Program & Molecular Therapies for Inborn Errors of Metabolism-Frontier Program to S.R., R01-HL164633 grant to P.K., and grant R38-HL143613-04 to S.N.H.; Calliope Joy Foundation to S.R.; and A.V. Kamens chair in translational neurotherapeutics to A.V.

AUTHOR CONTRIBUTIONS

L.T. is responsible for the majority of intellectual contribution, writing, and execution of a majority of the molecular biology, mouse transplant/sacrifice, and behavioral work conducted. S.S. made major contributions to the histopathology and gave key support for behavioral assays. J.L.H. made key contributions for mouse sacrifice, fixation, and histopathology. V.P. aided in mouse harvests. M.C. made intellectual contributions in LV design. L.B. aided in experimental design and execution. S.N.H. made major contributions to the EV work conceptualization and execution. N.T. made contributions to sample handling, colony-formation assay, and ddPCR. C.C.C. analyzed flow data for secondary transplants. M.H., A.R., J.E., and F.B. All contributed to the sequencing and alignment of the EA1 viral vector. A.G. analyzed flow data. Z.H. analyzed histopathology data. L.S. made intellectual contributions related to MLD disease biochemistry. K.R. made intellectual contributions related to MLD disease biochemistry. P.K. made intellectual contributions related to EV and LV work. R.A.-N. made intellectual contributions related to MLD disease treatment. L.A.A. is a major clinical contributor and collaborator for usage of our LV strategy in clinic. A.L.V. is a major clinical contributor and collaborator for usage of our LV strategy in clinic. S.R. is laboratory PI, prime intellectual contributor, and CO for the project.

DECLARATION OF INTERESTS

S.R. is a scientific advisory board member of Ionis Pharmaceuticals, Vifor, and Disc Medicine. Present to last 5 years: S.R. has been or is a consultant for GSK, BMS, Incyte, Cambridge Healthcare Res, Celgene Corporation, Catenion, First Manhattan Co., FORMA Therapeutics, Ghost Tree Capital, Keros Therapeutics, Noble insight, Protagonist Therapeutics, Sanofi Aventis U.S., Slingshot Insight, Spexis AG, Techspert.io, BVF Partners L.P., Rallybio LLC, venBio Select LLC, ExpertConnect LLC, and LifeSci Capital. The vector EA1 is protected in the patent-CHOP 2022-023: "Novel lentiviral vectors for the treatment of Multiple Sulfatase Deficiency (MSD), Metachromatic Leukodystrophy (MLD) and related disorder of sulfatase deficiency" (CHOP, L.T. and S.R.).

SUPPLEMENTAL INFORMATION

Supplemental information can be found online at https://doi.org/10.1016/j.omtn.2025.102464.

REFERENCES

1. Rosenberg, J.B., Kaminsky, S.M., Aubourg, P., Crystal, R.G., and Sondhi, D. (2016). Gene therapy for metachromatic leukodystrophy. J. Neurosci. Res. *94*, 1169–1179.
2. Brimley, C.J., Lopez, J., van Haren, K., Wilkes, J., Sheng, X., Nelson, C., Korgenski, E.K., Srivastava, R., and Bonkowsky, J.L. (2013). National variation in costs and mortality for leukodystrophy patients in US children's hospitals. Pediatr. Neurol. *49*, 156–162.e1.
3. Papaioannou, I., Owen, J.S., and Yáñez-Muñoz, R.J. (2023). Clinical applications of gene therapy for rare diseases: A review. Int. J. Exp. Pathol. *104*, 154–176.
4. Matzner, U., Breiden, B., Schwarzmann, G., Yaghootfam, A., Fluharty, A.L., Hasilik, A., Sandhoff, K., and Gieselmann, V. (2009). Saposin B-dependent reconstitution of arylsulfatase A activity in vitro and in cell culture models of metachromatic leukodystrophy. J. Biol. Chem. *284*, 9372–9381.
5. Schmidt, J.L., Pizzino, A., Nicholl, J., Foley, A., Wang, Y., Rosenfeld, J.A., Mighion, L., Bean, L., da Silva, C., Cho, M.T., et al. (2020). Estimating the relative frequency of leukodystrophies and recommendations for carrier screening in the era of next-generation sequencing. Am. J. Med. Genet. *182*, 1906–1912.
6. Farah, M.H., Dali, C.Í., Groeschel, S., Moldovan, M., Whiteman, D.A.H., Malanga, C.J., Krägeloh-Mann, I., Li, J., Barton, N., and Krarup, C. (2024). Effects of sulfatide on peripheral nerves in metachromatic leukodystrophy. Ann. Clin. Transl. Neurol. *11*, 328–341.
7. Fumagalli, F., Calbi, V., Natali Sora, M.G., Sessa, M., Baldoli, C., Rancoita, P.M.V., Ciotti, F., Sarzana, M., Fraschini, M., Zambon, A.A., et al. (2022). Lentiviral haematopoietic stem-cell gene therapy for early-onset metachromatic leukodystrophy: long-term results from a non-randomised, open-label, phase 1/2 trial and expanded access. Lancet *399*, 372–383.
8. Biffi, A., Capotondo, A., Fasano, S., del Carro, U., Marchesini, S., Azuma, H., Malaguti, M.C., Amadio, S., Brambilla, R., Grompe, M., et al. (2006). Gene therapy of metachromatic leukodystrophy reverses neurological damage and deficits in mice. J. Clin. Invest. *116*, 3070–3082.
9. Biffi, A., Montini, E., Lorioli, L., Cesani, M., Fumagalli, F., Plati, T., Baldoli, C., Martino, S., Calabria, A., Canale, S., et al. (2013). Lentiviral hematopoietic stem cell gene therapy benefits metachromatic leukodystrophy. Science *341*, 1233158.
10. Sessa, M., Lorioli, L., Fumagalli, F., Acquati, S., Redaelli, D., Baldoli, C., Canale, S., Lopez, I.D., Morena, F., Calabria, A., et al. (2016). Lentiviral haemopoietic stem-cell gene therapy in early-onset metachromatic leukodystrophy: an ad-hoc analysis of a non-randomised, open-label, phase 1/2 trial. Lancet *388*, 476–487.
11. Biffi, A., De Palma, M., Quattrini, A., Del Carro, U., Amadio, S., Visigalli, I., Sessa, M., Fasano, S., Brambilla, R., Marchesini, S., et al. (2004). Correction of metachromatic leukodystrophy in the mouse model by transplantation of genetically modified hematopoietic stem cells. J. Clin. Invest. *113*, 1118–1129.
12. Ginhoux, F., and Prinz, M. (2015). Origin of microglia: current concepts and past controversies. Cold Spring Harb. Perspect. Biol. *7*, a020537.
13. Schoenmakers, D.H., Mochel, F., Adang, L.A., Boelens, J.J., Calbi, V., Eklund, E.A., Grønborg, S.W., Fumagalli, F., Groeschel, S., Lindemans, C., et al. (2024). Inventory of current practices regarding hematopoietic stem cell transplantation in metachromatic leukodystrophy in Europe and neighboring countries. Orphanet J. Rare Dis. *19*, 46.
14. Kolata, G.. Sickle cell gene therapy trial halted after two patients develop cancer, though the link is not certain. Genetic Literacy Project. https://geneticliteracyproject.org/2021/03/03/sickle-cell-gene-therapy-trial-halted-after-two-patients-develop-cancer-though-the-link-is-not-certain/.
15. MARAC. Temporary Suspension of Clinical Trials. https://www.sicklecelldisease.org/2021/03/02/marac-statement-temporary-suspension-of-clinical-trials/.
16. Wakabayashi-Ito, N., and Nagata, S. (1994). Characterization of the regulatory elements in the promoter of the human elongation factor-1 alpha gene. J. Biol. Chem. *269*, 29831–29837.
17. Qin, J.Y., Zhang, L., Clift, K.L., Hulur, I., Xiang, A.P., Ren, B.Z., and Lahn, B.T. (2010). Systematic comparison of constitutive promoters and the doxycycline-inducible promoter. PLoS One *5*, e10611.
18. Kim, D.W., Uetsuki, T., Kaziro, Y., Yamaguchi, N., and Sugano, S. (1990). Use of the human elongation factor 1 alpha promoter as a versatile and efficient expression system. Gene *91*, 217–223.
19. Breda, L., Ghiaccio, V., Tanaka, N., Jarocha, D., Ikawa, Y., Abdulmalik, O., Dong, A., Casu, C., Raabe, T.D., Shan, X., et al. (2021). Lentiviral vector ALS20 yields high hemoglobin levels with low genomic integrations for treatment of beta-globinopathies. Mol. Ther. *29*, 1625–1638.
20. Zufferey, R., Donello, J.E., Trono, D., and Hope, T.J. (1999). Woodchuck hepatitis virus posttranscriptional regulatory element enhances expression of transgenes delivered by retroviral vectors. J. Virol. *73*, 2886–2892.
21. Rivella, S., Callegari, J.A., May, C., Tan, C.W., and Sadelain, M. (2000). The cHS4 insulator increases the probability of retroviral expression at random chromosomal integration sites. J. Virol. *74*, 4679–4687.
22. Browning, D.L., Everson, E.M., Leap, D.J., Hocum, J.D., Wang, H., Stamatoyannopoulos, G., and Trobridge, G.D. (2017). Evidence for the in vivo safety of insulated foamy viral vectors. Gene Ther. *24*, 187–198.
23. Browning, D.L., and Trobridge, G.D. (2016). Insulators to Improve the Safety of Retroviral Vectors for HIV Gene Therapy. Biomedicines *4*, 4.
24. Romero, Z., Campo-Fernandez, B., Wherley, J., Kaufman, M.L., Urbinati, F., Cooper, A.R., Hoban, M.D., Baldwin, K.M., Lumaquin, D., Wang, X., et al. (2015). The human ankyrin 1 promoter insulator sustains gene expression in a beta-globin lentiviral vector in hematopoietic stem cells. Mol. Ther. Methods Clin. Dev. *2*, 15012.
25. Browning, D.L., Collins, C.P., Hocum, J.D., Leap, D.J., Rae, D.T., and Trobridge, G.D. (2016). Insulated Foamy Viral Vectors. Hum. Gene Ther. *27*, 255–266.
26. Kingsman, S.M., Mitrophanous, K., and Olsen, J.C. (2005). Potential oncogene activity of the woodchuck hepatitis post-transcriptional regulatory element (WPRE). Gene Ther. *12*, 3–4.
27. Skarpidi, E., Vassilopoulos, G., Stamatoyannopoulos, G., and Li, Q. (1998). Comparison of expression of human globin genes transferred into mouse erythroleukemia cells and in transgenic mice. Blood *92*, 3416–3421.

28. Domingues, H.S., Portugal, C.C., Socodato, R., and Relvas, J.B. (2016). Oligodendrocyte, Astrocyte, and Microglia Crosstalk in Myelin Development, Damage, and Repair. Front. Cell Dev. Biol. *4*, 71.

29. Wolf, N.I., Breur, M., Plug, B., Beerepoot, S., Westerveld, A.S.R., van Rappard, D.F., de Vries, S.I., Kole, M.H.P., Vanderver, A., van der Knaap, M.S., et al. (2020). Metachromatic leukodystrophy and transplantation: remyelination, no cross-correction. Ann. Clin. Transl. Neurol. *7*, 169–180.

30. Do, M.A., Levy, D., Brown, A., Marriott, G., and Lu, B. (2019). Targeted delivery of lysosomal enzymes to the endocytic compartment in human cells using engineered extracellular vesicles. Sci. Rep. *9*, 17274.

31. Hurwitz, S.N., Olcese, J.M., and Meckes, D.G., Jr. (2019). Extraction of Extracellular Vesicles from Whole Tissue. J. Vis. Exp. https://doi.org/10.3791/59143.

32. Hurwitz, S.N., and Meckes, D.G., Jr. (2017). An Adaptable Polyethylene Glycol-Based Workflow for Proteomic Analysis of Extracellular Vesicles. Methods Mol. Biol. *1660*, 303–317.

33. Ikawa, Y., Uchiyama, T., Jagadeesh, G.J., and Candotti, F. (2016). The long terminal repeat negative control region is a critical element for insertional oncogenesis after gene transfer into hematopoietic progenitors with Moloney murine leukemia viral vectors. Gene Ther. *23*, 815–818.

34. Ory, D.S., Neugeboren, B.A., and Mulligan, R.C. (1996). A stable human-derived packaging cell line for production of high titer retrovirus/vesicular stomatitis virus G pseudotypes. Proc. Natl. Acad. Sci. USA *93*, 11400–11406.

35. Matzner, U., and Gieselmann, V. (2005). Gene therapy of metachromatic leukodystrophy. Expert Opin. Biol. Ther. *5*, 55–65.

36. SERVICK, K. (2021). Gene therapy clinical trial halted as cancer risk surfaces. Science. https://www.science.org/content/article/gene-therapy-clinical-trial-halted-cancer-risk-surfaces.

37. Goodman, M.A., Arumugam, P., Pillis, D.M., Loberg, A., Nasimuzzaman, M., Lynn, D., van der Loo, J.C.M., Dexheimer, P.J., Keddache, M., Bauer, T.R., Jr., et al. (2018). Foamy Virus Vector Carries a Strong Insulator in Its Long Terminal Repeat Which Reduces Its Genotoxic Potential. J. Virol. *92*, e01639-17.

38. Ferreira, M.V., Cabral, E.T., and Coroadinha, A.S. (2021). Progress and Perspectives in the Development of Lentiviral Vector Producer Cells. Biotechnol. J. *16*, e2000017.

39. Thielen, F.W., Heine, R.J.S.D., Berg, S.V.D., Ham, R.M.T.T., and Groot, C.A.U.d. (2022). Towards sustainability and affordability of expensive cell and gene therapies? Applying a cost-based pricing model to estimate prices for Libmeldy and Zolgensma. Cytotherapy *24*, 1245–1258.

40. Cornetta, K., Bonamino, M., Mahlangu, J., Mingozzi, F., Rangarajan, S., and Rao, J. (2022). Gene therapy access: Global challenges, opportunities, and views from Brazil, South Africa, and India. Mol. Ther. *30*, 2122–2129.

41. Jelin, A.C., and Vora, N. (2018). Whole Exome Sequencing: Applications in Prenatal Genetics. Obstet. Gynecol. Clin. North Am. *45*, 69–81.

42. Dukhovny, S., and Norton, M.E. (2018). What are the goals of prenatal genetic testing? Semin. Perinatol. *42*, 270–274.

43. Marks, P.A., and Rifkind, R.A. (1978). Erythroleukemic differentiation. Annu. Rev. Biochem. *47*, 419–448.

44. Baum, H., Dodgson, K.S., and Spencer, B. (1959). The assay of arylsulphatases A and B in human urine. Clin. Chim. Acta *4*, 453–455.

45. Pare, B., Deschenes, L.T., Pouliot, R., Dupre, N., and Gros-Louis, F. (2016). An Optimized Approach to Recover Secreted Proteins from Fibroblast Conditioned-Media for Secretomic Analysis. Front. Cell. Neurosci. *10*, 70.

46. Rider, M.A., Hurwitz, S.N., and Meckes, D.G., Jr. (2016). ExtraPEG: A Polyethylene Glycol-Based Method for Enrichment of Extracellular Vesicles. Sci. Rep. *6*, 23978.

47. Kowal, J., Arras, G., Colombo, M., Jouve, M., Morath, J.P., Primdal-Bengtson, B., Dingli, F., Loew, D., Tkach, M., and Théry, C. (2016). Proteomic comparison defines novel markers to characterize heterogeneous populations of extracellular vesicle subtypes. Proc. Natl. Acad. Sci. USA *113*, E968–E977.

48. Hurwitz, S.N., Sun, L., Cole, K.Y., Ford, C.R., 3rd, Olcese, J.M., and Meckes, D.G., Jr. (2018). An optimized method for enrichment of whole brain-derived extracellular vesicles reveals insight into neurodegenerative processes in a mouse model of Alzheimer's disease. J. Neurosci. Methods *307*, 210–220.

49. Sase, S., Almad, A.A., Boecker, C.A., Guedes-Dias, P., Li, J.J., Takanohashi, A., Patel, A., McCaffrey, T., Patel, H., Sirdeshpande, D., et al. (2020). TUBB4A mutations result in both glial and neuronal degeneration in an H-ABC leukodystrophy mouse model. Elife *9*, e52986.